VTEC observations of intense geomagnetic storms above Nepal: comparison with satellite data, CODE and IGSG models

D. Pandit, Christine Amory-Mazaudier, R. Fleury, N P Chapagain, B. Adhikari

▶ **To cite this version:**

D. Pandit, Christine Amory-Mazaudier, R. Fleury, N P Chapagain, B. Adhikari. VTEC observations of intense geomagnetic storms above Nepal: comparison with satellite data, CODE and IGSG models. Indian Journal of Physics, 2022, 10.1007/s12648-022-02441-w . hal-03791229

HAL Id: hal-03791229
https://hal.science/hal-03791229

Submitted on 29 Sep 2022

HAL is a multi-disciplinary open access archive for the deposit and dissemination of scientific research documents, whether they are published or not. The documents may come from teaching and research institutions in France or abroad, or from public or private research centers.

L'archive ouverte pluridisciplinaire **HAL**, est destinée au dépôt et à la diffusion de documents scientifiques de niveau recherche, publiés ou non, émanant des établissements d'enseignement et de recherche français ou étrangers, des laboratoires publics ou privés.

Indian J Phys
https://doi.org/10.1007/s12648-022-02441-w

ORIGINAL PAPER

VTEC observations of intense geomagnetic storms above Nepal: comparison with satellite data, CODE and IGSG models

D Pandit[1,6]*, C Amory-Mazaudier[2,3], R Fleury[4], N P Chapagain[5] and B Adhikari[6]

[1]Central Department of Physics, IOST, Tribhuvan University, Kathmandu, Nepal

[2]LPP, Polytechnique, Sorbonne Universités UPMC Paris 06, Paris, France

[3]T/ICT4D, Abdus Salam ICTP, Trieste, Italy

[4]Lab-STICC, UMR 6285, Institut Mines-Telecom Atlantique, Site de Brest, France

[5]Amrit Campus, Tribhuvan University, Thamel, Kathmandu, Nepal

[6]Department of Physics, St. Xavier's College, Maitighar, Kathmandu, Nepal

Received: 28 October 2021 / Accepted: 26 July 2022

Abstract: In this article, we analyze vertical total electron content (VTEC) over Nepal for 4 periods: March 14–25, 2015, June 18–29, 2015, May 24–June 4, 2017, and September 3–14, 2017. In each period, there are quiet geomagnetic days and intense geomagnetic stormy days. The VTEC observed during these periods has observed both positive and negative ionospheric storms. We compared VTEC Receiver-Independent Exchange Format (RINEX) observations with the Global Ionospheric Map (GIM), Centre for Orbit Determination in Europe (CODE), and IGS working group (IGSG). We found in RINEX observation of the VTEC a noon bite out profile with predominance of morning and afternoon peaks and a nighttime peak, but this was not noticeable clearly with CODE and IGSG models. The comparison between RINEX TEC, CODE, and IGSG models shows that the GIM model does not estimate RINEX VTEC over Nepal. The disagreement between VTEC CODE/IGSG and VTEC RINEX is important during geomagnetically quiet periods, while there is good agreement between VTEC CODE/IGSG and VTEC RINEX during strong geomagnetic storms. We also find a greater disagreement between the models and the data at the equinoxes when the VTEC is larger. It is, therefore, necessary to introduce data from Nepal stations into the models CODE and IGSG in order to improve them.

Keywords: Total electron content (TEC); Geomagnetic storms; Global Ionospheric Map (GIM); Receiver-Independent Exchange Format (RINEX) data; UNAVCO

1. Introduction

Gonzalez et al. [1] in their article title, 'What is a geomagnetic storm?', defined the two essential parameters, which are the Bz component of the interplanetary magnetic field (IMF) and the magnetic storm index Dst [2], which is the signature of the ring current circulating in the magnetosphere. Gonzales et al. [1] classified the magnetic storms in three classes: weak (-30 nT $<$ Dst <-50 nT), moderate (-50 nT $<$ Dst <-100 nT), and strong (Dst <-100nT). When the IMF-Bz is southward, in the opposite direction of the Earth's magnetic field, there is the reconnection between the IMF and the Earth's magnetic field [3] and an important amount of energy is transferred from the interplanetary medium to the magnetosphere. The auroral zone is directly impacted. Electric fields and electric currents are increased and create Joule heating at the origin of the thermal expansion of the atmosphere, leading to changes in temperatures, motions, and composition. There are also precipitations of the particle in the ionosphere as well as field aligned currents connecting the magnetosphere and ionosphere [4].

Three main physical processes are known to act at planetary scale via electrodynamics coupling between the auroral zone and the middle and low latitudes:

*Corresponding author, E-mail: drabindrapandit087@gmail.com

Published online: 23 August 2022

© 2022 IACS

(1) There is the thermal expansion of the atmosphere with mass transport between the pole and the equator. This process, linked to Joule heating in the auroral zone, not only modifies temperatures, pressures, and motions but also chemistry and causes changes in the composition of the atmosphere, as theorized by Fuller-Rowell et al. [5, 6].
(2) There is the extension of the electric field of magnetospheric convection from the auroral zone to low latitudes, as theorized first by Vasyliunas [7].
(3) There is also the process of the disturbed ionospheric dynamo linked to the Joule heating, which creates a disturbance of the thermospheric winds, in turn generating disturbed electric fields and currents at medium and low latitudes, as theorized first by Blanc and Richmond [8]. These pioneering theoretical works made it possible to understand the influence of each physical process. Currently, numerical simulations with physical planetary models integrated many physical processes (Thermosphere-Ionosphere-Electrodynamics Global Circulation Model [TIEGCM] https://www.hao.ucar.edu/modeling/tgcm/, Coupled Thermosphere/Ionosphere Plasmasphere [CTIP] https://ccmc.gsfc.nasa.gov/modele/ctip.php).

This makes it possible to study the evolution of geophysical parameters during geomagnetic storm. For several decades, Global Navigation Satellite System (GNSS) and, in particular, Global Positioning System (GPS) allowed the measurement of the number of electrons (Total Electron Content, TEC) that the satellite signal encounters during its path between the satellite and receivers on the Earth. TEC is mainly due to the electrons of the ionosphere, and therefore, the analysis of TEC allows us to study the variations of ionospheric ionization during geomagnetic storms. TEC allows observing positive ionospheric storms (an increase in TEC) or negative ionospheric storms (a decrease in TEC).

In Nepal, there is a network of more than ten GPS stations (https://www.unavco.org), some of which have been operating for more than one solar cycle. Network of GPS stations in Nepal was installed by UNAVCO to study the seismicity of the region (out of the scope of this paper). Since several years, the Nepalese network of GPS has been used for the study of the ionosphere and space weather.

Huang et al. [9] used GPS data of Nepal to measure ground deformation caused by the 2015 Nepal earthquake. Adhikari et al. [10] studied the seismogenic energy deposited during the Nepal earthquake (April 25, 2015) using GPS network data from Nepal. Ansari et al. [11] studied TEC during the low solar activity year of 2017 over Nepal and found that the singular spectral analysis (SSA) method could be a more successful tool for forecasting the TEC over Nepal than the Global Ionospheric Maps (GIMs) and International Reference Ionosphere extended to Plasmasphere (IRI-Plas) 2017. A model using an empirical orthogonal function was developed by Jamjareegulgarn et al. [12] to forecast TEC over Nepal. The climatology of TEC over Nepal was studied by Pandit et al. [13] using a solar cycle GPS data.

Our article is in the framework of space weather. We first analyze the Physics of the phenomena disturbing the ionosphere, and in particular, the TEC, which allows correct satellite positioning. Then we compare our TEC observations to the TEC maps for different conditions of geomagnetic activity in order to understand the effect of geomagnetic activity. We think that it is important to analyze the Physics to see in which cases the maps are worthy. These maps are produced to assist users, and we believe our study may help to improve them. Precisely, in this paper, we studied the impact of four intense geomagnetic storms (March 2015, June 2015, May 2017, and September 2017) of solar cycle 24 on VTEC data from Nepalese stations, and for the first time, we compared our observations to the Centre for Orbit Determination in Europe (CODE) and the IGS working group (IGSG) mapping models. Section 2 is devoted to the data set and data processing. Section 3 presents an analysis of storms. In Sect. 4, we compare the VTEC observations to the VTEC given by the mapping models, and then we conclude the results in Sect. 5.

2. Data sets, data processing, and models

2.1. Data sets

Different sources of data sets are used to characterize the intense storm of solar cycle 24.

The data sets from the ACE (Advanced Composition Explorer, www.srl.caltech.edu/ACE/) satellites are used to provide information on the key parameters of the solar wind, such as the southward component of the interplanetary magnetic field (IMF-Bz) and the solar wind velocity.

The magnetic indices SYM-H measure the intensity of the storm time ring current and the AE index provides a quantitative measure of magnetic activity and energy deposited in the auroral zone. The data sets for these indices were obtained from the website http://www.omniweb.gsfc. The data set for the Polar Cap magnetic index (PC index), which measures of the merging electric field at the polar region, was downloaded from http://www.isgi.unistra.fr/.

The behavior of the ionospheric response during the four storms, March 14–25, 2015, June 18–29, 2015, May 24–June 4, 2017, and September 3–14, 2017, over Nepal is

studied by using VTEC computed by the Fleury's software (MATLAB programming on www.girgea.org). The RINEX data file for GPS TEC is extracted from http://www.unavco.org. Figure 1 presents a map of Nepal with the locations of the GPS network and the stations used for this study, and Table 1 gives their geographic and geomagnetic coordinates.

We used the thermospheric O/N_2 ratio obtained from the website http://guvitimed.jhuapl.edu/ to compare the effect of storms on the ground-based GPS TEC and satellite data on the O/N_2 ratio.

2.2. Data processing—VTEC (Fleury's method)

The computation of VTEC is based on the standard procedure used for processing GPS pseudo-range measurements [14, 15]. For the conversion of Slant TEC (STEC) to vertical TEC (VTEC), we use the single-layer mapping function (MF) at 420 km [15, 16]. The STEC is conventionally calculated by the combination of the two dual-frequency pseudo-range measurements available on the daily RINEX 30 s files. Satellite differential code bias (DCB) is corrected using values provided by the CODE organization at the University of Bern. The receiver bias is calculated using the GIM/CODE model on the Pierce points with an elevation angle ε greater than 30°. This limit eliminates distant points where the horizontal gradient could become significant and data affected by multipath. The STEC estimate is based on the ionospheric MF, where a is the Earth's radius (6371.2 km) and h_m, a reference altitude, has been taken at 420 km.

$$\mathrm{MF} = \sqrt{1 - \left(\frac{a * \cos(\varepsilon)}{a + h_m}\right)^2}$$

The adjustment of the two STECs thus calculated (one from the RINEX data and the second from the GIM model) makes it possible to obtain the unknown daily DCB of the receiver. The VTEC above the receiver is obtained by a least-square regression weighted by the inverse of the square of the distance to the Pierce point over a time interval of 15 min.

2.3. MODELS CODE and IGSG

2.3.1. CODE

Since the creation of the International GPS Service (IGS) scientific community in 1998, several organizations (CODE, European Space Agency [ESA], Jet Propulsion Laboratory [JPL], Universitat Politècnica de Catalunya [UPC]) have created an ionosphere working group (IONO-WG) to produce global and daily VTEC maps using the ground station network. A standard writing format, IONEX (for IONosphere Map Exchange), has been adopted, providing the VTEC on a regular grid in 2.5° latitude and 5° longitude. Only the temporal rate has changed over time: every 2 h and then 1 h with daily continuity (and 15 min for rapid Universitat Politècnica de Catalunya Rapid GIM [UQRG]). One of the major difficulties lies in the

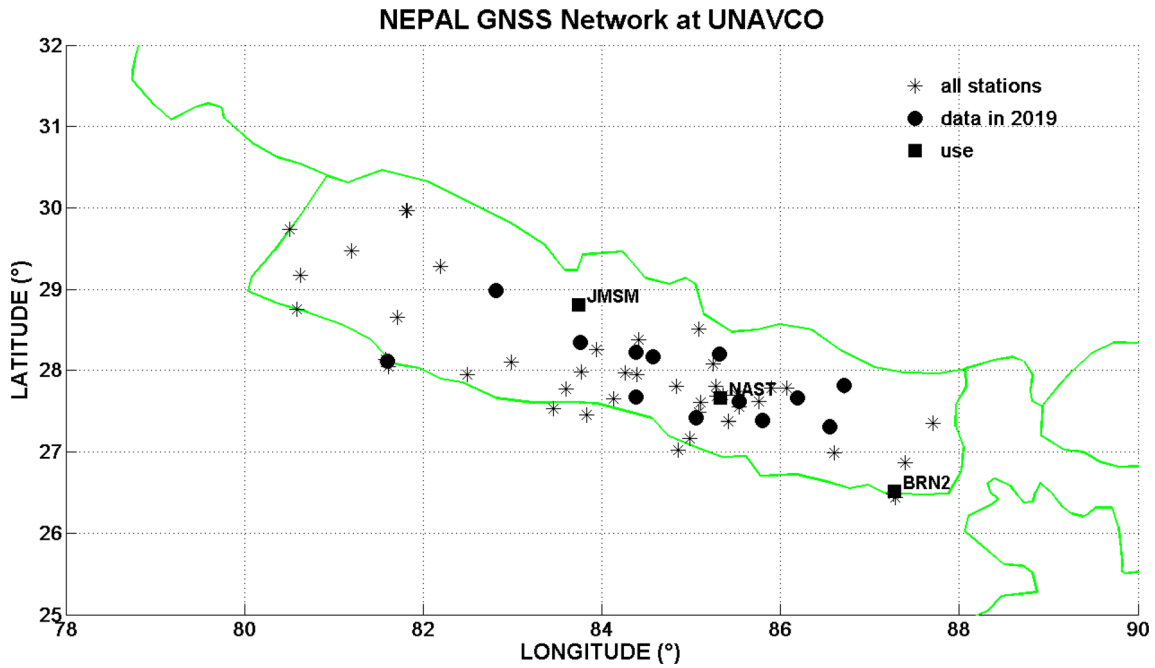

Fig. 1 A map of Nepal showing locations of GPS network and the stations used in our study

Table 1 Geographic and geomagnetic coordinates of GPS stations

Locations of GPS stations	ID	Geog. Lat.	Geog. Long.	Geom. Lat.	Geom. Long.	Dip Lat.	Local time (LT)
Biratnagar, Nepal	BRN2	26.51° N	87.27° E	17.22° N	161.19° E	41.56	UT + 5:45 h
Kathmandu, Nepal	NAST	27.65° N	85.32° E	17.47° N	169.37° E	43.61	UT + 5:45 h
Jomsom, Nepal	JMSM	28.80° N	83.74° E	19.70° N	150.05° E	45.31	UT + 5:45 h

determination of Differential Code Biases (DCB) on satellites, but especially on ground stations that involve different manufacturers and environmental changes. According to the organizations, different methods of developing STEC in VTEC have been used: Spherical Harmonics (CODE, ESA, Wuhan University [WHU], Chinese Academy of Sciences [CAS]), three-shell model (JPL), and tomographic methods with splines (UPC). The performance of these models was evaluated on the basis of ancillary measures of altimeters and radio occultation [17, 18]. GIM maps gain in quality with the increase in the number of ground stations (more than 500 currently) and the integration of new navigation systems (Glonass, Galileo, and Beidou). The difference between the estimations given by the GIM maps and the observations is of the order of 2 TECU during the sunspot minimum and can reach 10 TECU in the years of the sunspot maximum [19, 20]. The GIM maps provided by CODE (http://www.aiub.unibe.ch/download/CODE) is to compare with GPS TEC derived from the RINEX observational file obtained from GPS stations in Nepal.

2.3.2. IGSG

In fact, there are many Ionosphere Associate Analysis Centers (IAACs) that produce GIMs from the IGS network stations. In each case, the mathematical methods are different, so the results are not the same. The 'ionosphere group' of the IGS (IONO-WG) under the current responsibility of A. Krankowski [17] was aware of the problem and proposed an algorithm to combine all these particular solutions into one solution labeled IGS (IGSG). The GIM maps provided by IGSG (https://cddis.nasa.gov/archive/gnss/products/ionex/) to compare GPS TEC are derived from the RINEX observational files obtained from GPS stations in Nepal.

3. Results and discussion

3.1. Global geophysical context

Figure 2(a), (b), (c), and (d) shows 1-min resolution of variations in the solar wind interplanetary plasma parameters, polar cap indices, and geomagnetic indices for the periods of March 14–24, 2015, June 18–28, 2015, May 24–June 3, 2017, and September 3–13, 2017, including a few days before and after the geomagnetic storm that occurred on March 17, 2015, June 22, 2015, May 27, 2017, and September 7, 2017, respectively. The first, second, third, fourth, fifth, and sixth panels in each plot show variations in solar wind velocity (Vx in km/s), interplanetary magnetic field (in nT), solar wind pressure (in nPa), polar cap north and south indices (PCN/PCS in mV/m), auroral indices (AE AU AL AO in nT), and SYM-H (in nT), respectively. The vertical dotted line in each figure represents the Sudden Storm Commencement (SSC). The horizontal lines with double arrow heads in each plot represent the main phase and the recovery phase during the geomagnetic storms.

The coronal mass election (CME) erupted from the magnetic filament on March 15, 2015, and reached on the Earth on March 17. The SSC is characterized by an abrupt enhancement in the positive value of SYM-H before the start of the main phase of the geomagnetic storm, as indicated in Fig. 2a by dotted vertical lines, and is observed at 04:45 UT followed by an increase in average solar wind speed from 420 to 500 km/s and solar wind pressure from 20 to 30 nPa. On March 20 and 21, the slight increase in solar wind speed is noticed due to coronal hole, which transfer additional momentum and energy at the time of the recovery phase, making it prolonged for 7 days. Coronal holes are the region of open field lines in the solar corona that act as efficient conduits for flushing heated plasma from the corona, energizing the solar wind, and prolonging the recovery phase of the storm for many days. The rapid southward and northward fluctuation in IMF Bz occurs during the storm with a minimum of − 20 nT. During the main phase at 20:30 UT, the SYM-H was noticed at about -132 nT and the minimum value of SYM-H noticed during this storm was < -200 nT. During the main phase of the storm, the decrease in H component is the signature of the intensification of westward ring current and increase in H component indicates slow recovery to normal phase on 18 March. The maximum value of AE noticed during this storm is 2000 nT and oscillating IMF-Bz at higher values of Vx is the signature of a high-speed streamer flowing around the Earth.

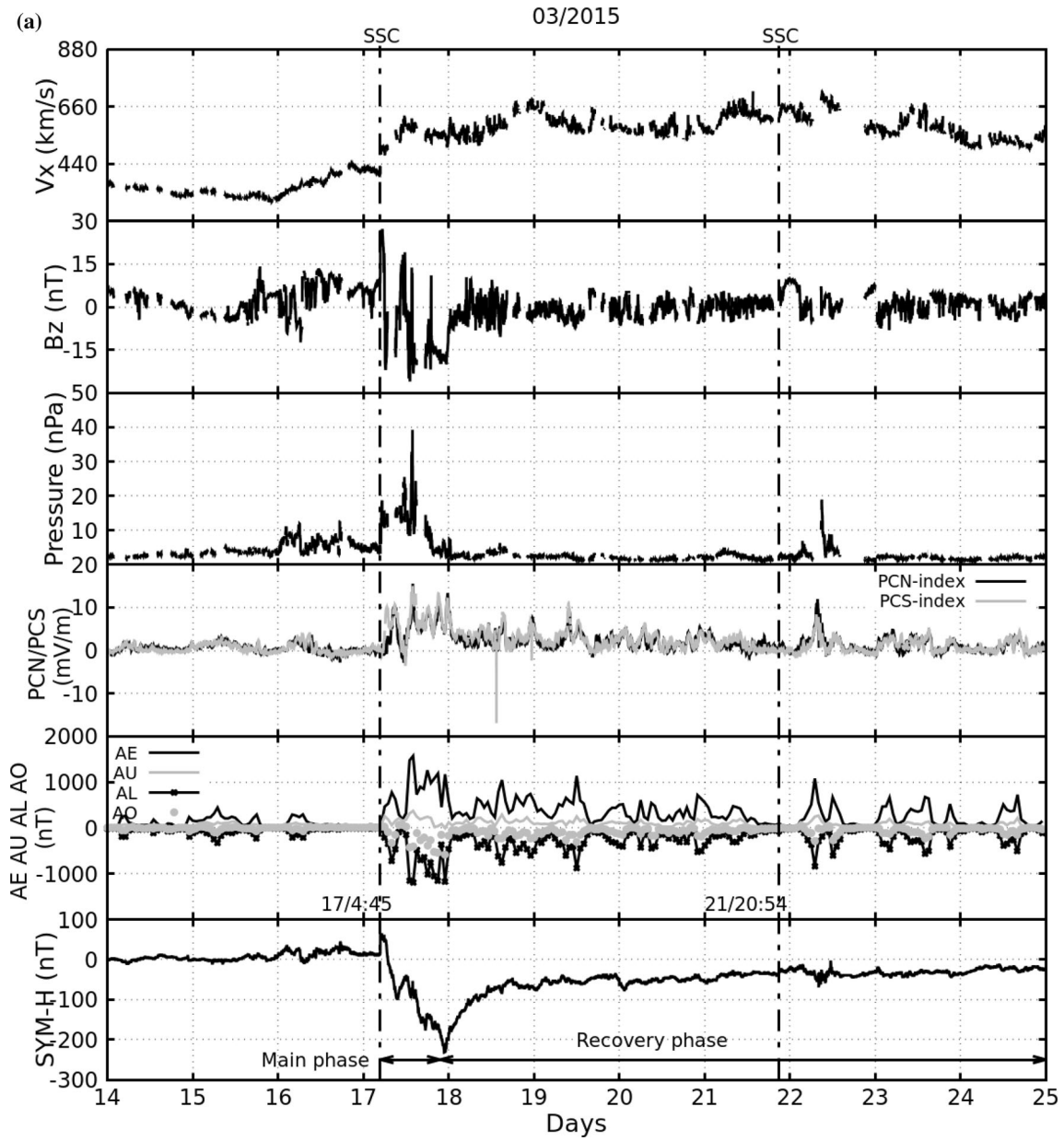

Fig. 2 (**a**–**d**) Variations of solar wind speed (Vx in km/s), interplanetary magnetic field IMF (Bz in nT), pressure (nPa), polar cap north (dark black curves) and south indices (faint black curves) in mV/m, auroral indices: AE (dark black curves), AU (faint black curves), AL (dark black curves with asterisk), AO (faint black doted curves) in nT, and SYM-H (nT) characterizing the geomagnetic storm during March 14–24, 2015, June 18–28, 2015, May 24–June3, 2017, and September 3–13, 2017, respectively. Vertical line in last panel represents sudden storm commencement and horizontal lines with double arrow heads represent the main and recovery phases

Likewise, for the storm of June 22, 2015, the three SSC were observed at 13:43 UT on June 21, 5:45 UT, and 18:33 UT on June 22, respectively. During the first, second, and third shocks, the solar wind speed increased from 300 to 350 km/s, 350 to 400 km/s, and 420 to 700 km/s, respectively. The maximum positive SYM-H during the first, second, and third shocks is 40 nT, $\sim$ 40 nT, and $\sim$ 90 nT, respectively. The main feature of this storm is the rapid, large-amplitude fluctuation of IMF Bz during its main and recovery phases. It was also observed with a minimum value of $-$ 37.6 nT at 19:20 UT on June 22. The AE value acquired during the main phase was 2300 nT. When the Bz has a negative value for a longer duration, the SYM-H reaches $-$ 200 nT at $\sim$ 5:30 UT on 23 June.

During the storm of May 27, 2017, an SSC was observed at 15:34 UT on May 27. The storm begins quietly, with sudden changes in solar wind speed ranging from 300 to 400 km/s and pressure ranging from 1 to 15 nPa. The main phase began on May 27; recovery on May 28, with a minimum Dst excursion to $-$ 125 nT, and the event

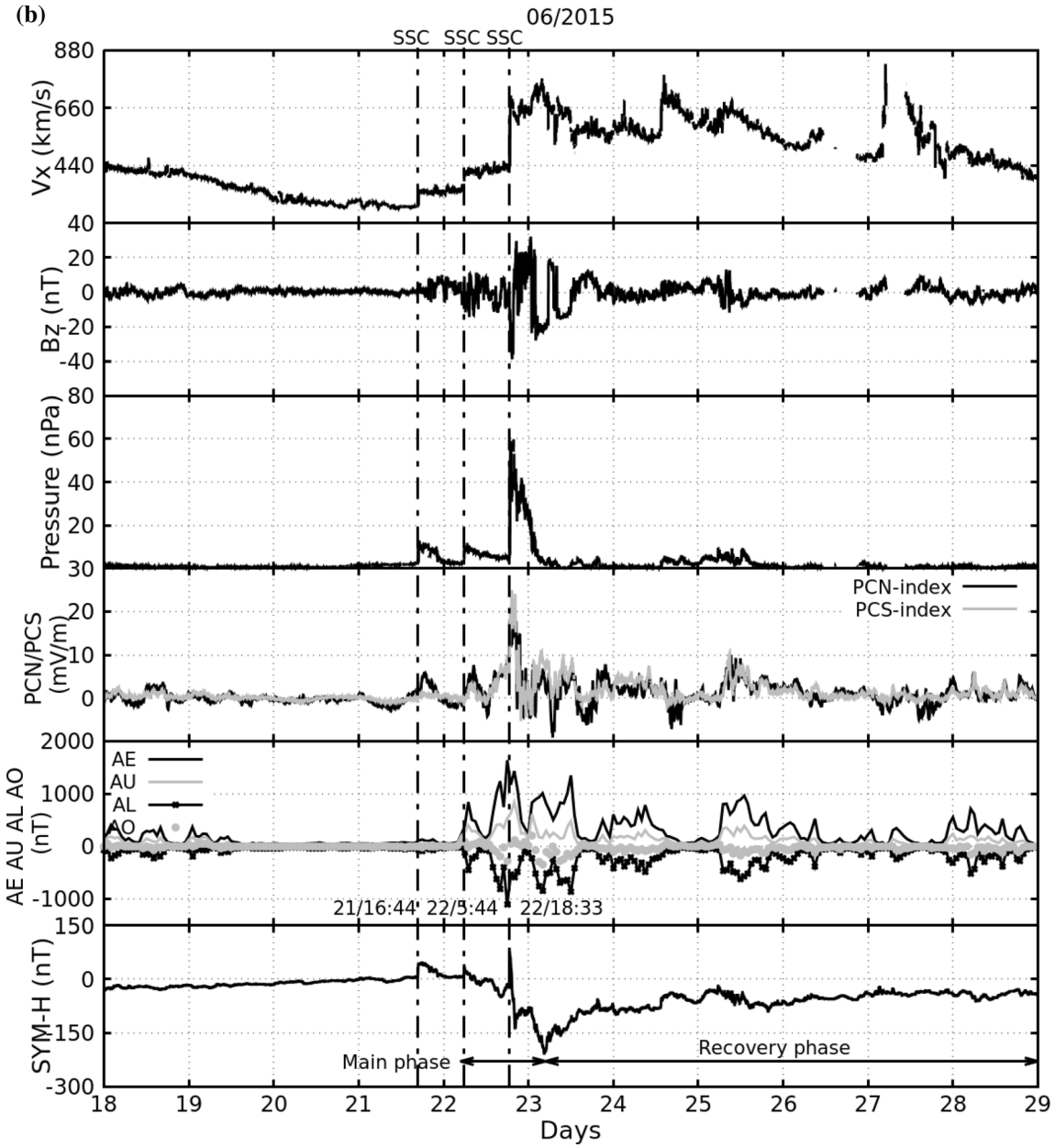

Fig. 2 continued

lasted until May 30, 2017. The maximum AE index was noticed $\sim$ 2000 nT with a minimum of IMF Bz ~ -18 nT on 28May.

During the storm of September 7, 2017, the first SSC was noticed on the 6th at 23:44 UT and the second, on the 7th at 23:00 UT. The first two significant minimums of SYM-H were observed on September 8 ($-$ 142 nT) at 02:00 UT and the second on September 8 ($-$ 122 nT) at 15:00 UT. The minimum value of SYM-H and the maximum bursts of AE do not coincide precisely in time. The maximum AE observed was 1300 nT and 1500 nT. The time lag between the minimum SYM-H and AE maxima was 3 h and 2 h earlier, respectively. The possible cause is that the geomagnetic disturbance shifted from higher latitudes to lower latitudes. Nevertheless, the PC bursts follow the same trend as the SYM-H minima. During the first and second strokes, the quick changes in the solar wind velocity and pressure were from 450 to 650 km/s and 600–850 km/s; 1 to 14 nPa and 1 to 10 nPa, respectively.

Table 2 summarizes the characteristics of the four storms studied.

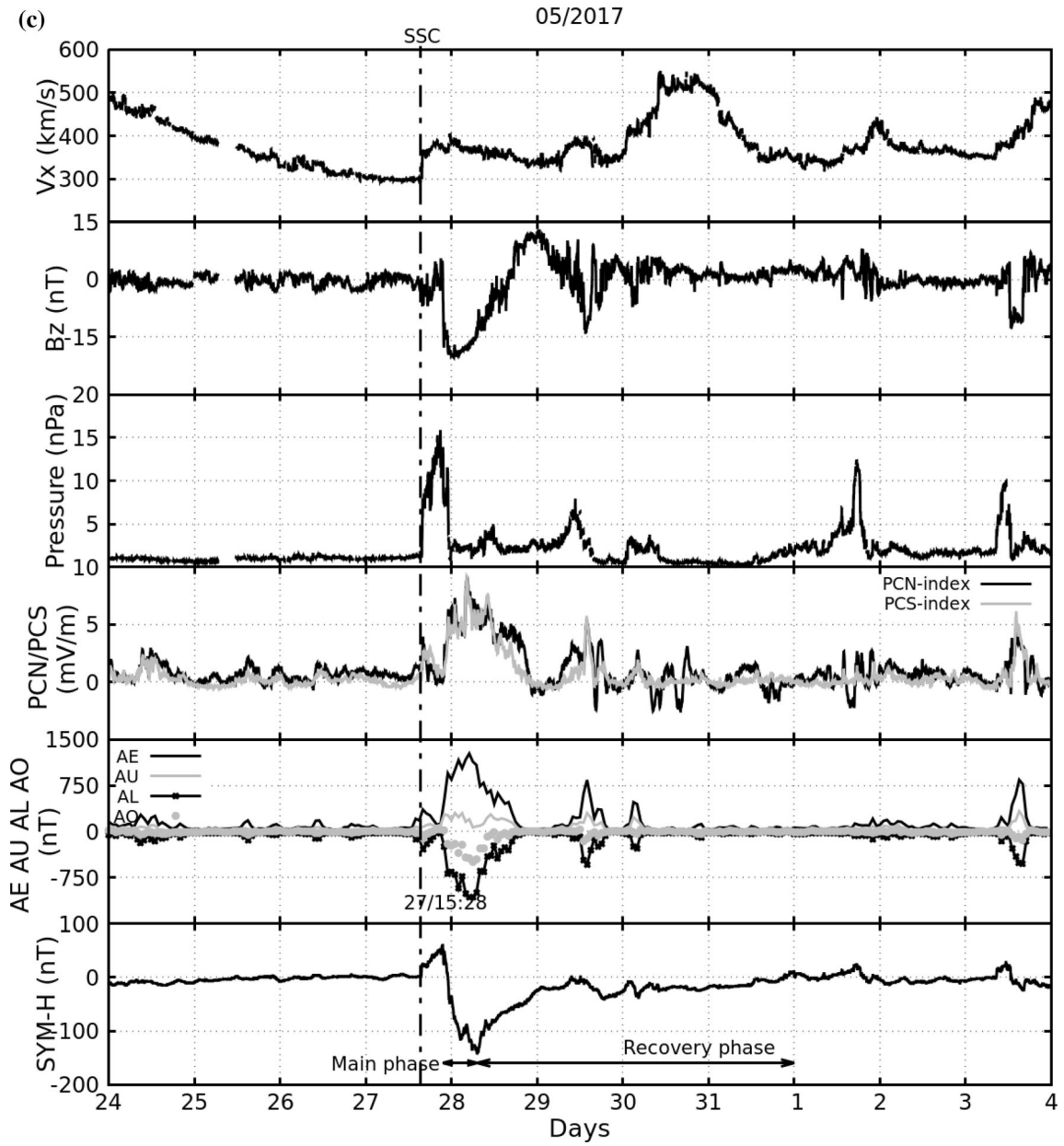

Fig. 2 continued

3.2. GPS VTEC

Figure 3(a), (b), (c), and (d) shows the temporal variation of VTEC during geomagnetic storms and geomagnetic quiet days, using GPS data from Nepal during March 14 to March 24, 2015, June 18 to June 28, 2018, May 24 to June 3, 2017, and September 3 to September 13, 2017, respectively. The first, second, and third panels in each figure represent the VTEC of stations BRN2, JMSM, and NAST in Nepal. The dotted black curve on each panel represents the average daily variation (a computed average of four days before the storm started). The quiet day variation is calculated from an average of data from March 13 to March 16, 2015, June 18 to June 21, 2015, May 23 to May 26, 2017, and September 3 to September 6, 2017 for the respective storms. The dark black curve indicates the variation in VTEC during storm time. The vertical line in each figure represents the SSC. The latitudinal (3°) and longitudinal (4°) distances between the selected stations are not very large; the electric field disturbances reach the daytime ionosphere at the same time, with similar intensity and duration. Hence, a marked latitudinal and longitudinal

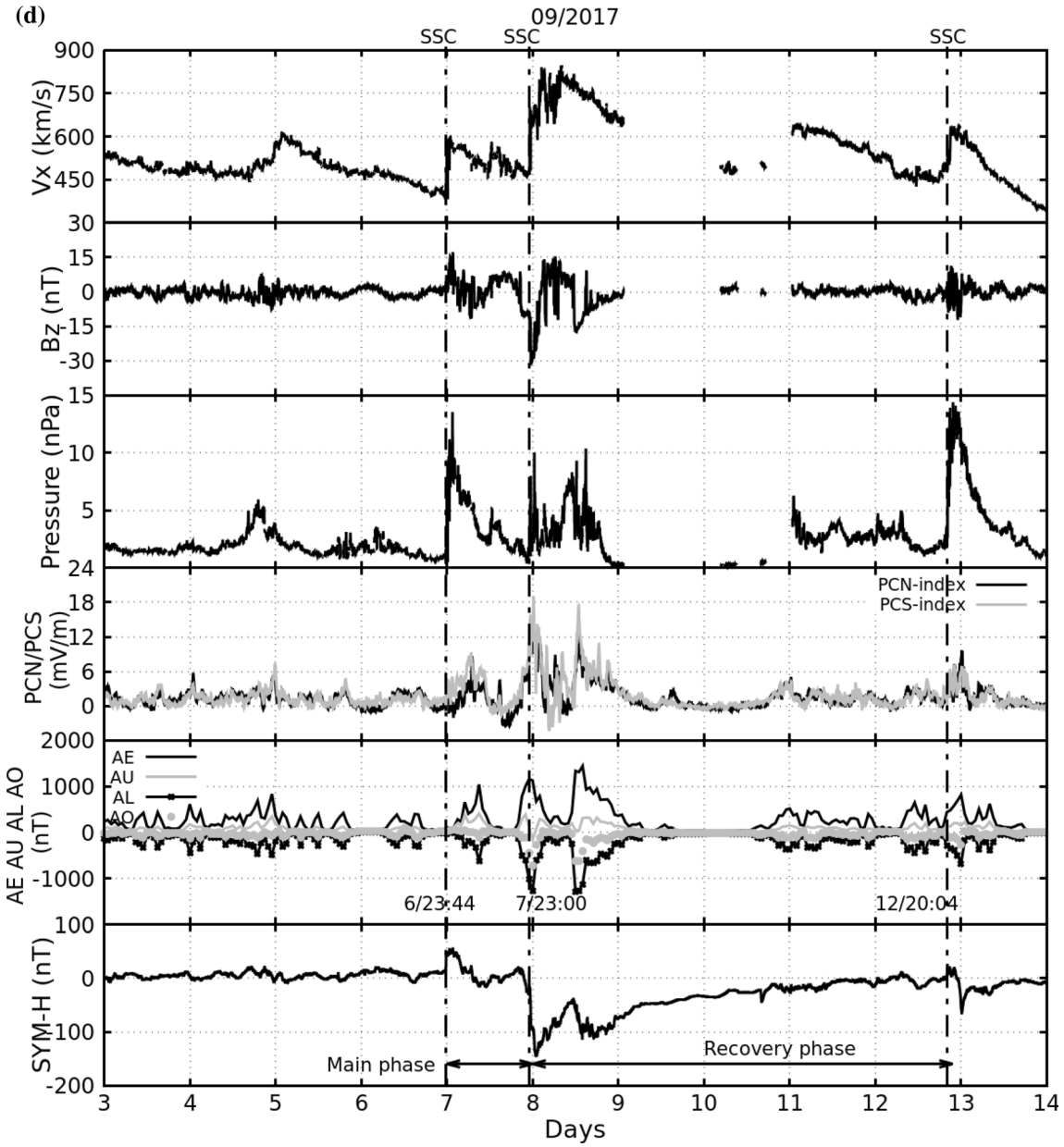

Fig. 2 continued

difference in the ionospheric response from these three stations is insignificant. In every station, a dome-shaped VTEC was observed. The trend of VTEC variation before the storm is almost similar to that of regular variation, but it gets disturbed when a geomagnetic storm starts.

The observations for each case of geomagnetic storms are as follows:

- *March 2015* The three days before the storm (14–16/03) are characterized by a similar dome-shaped diurnal variation with a maximum value of between 95 and 100 TECU. The onset of the magnetic storm was localized on 17/03 in the morning sector, and the diurnal maximum was observed at 90 TECU (Fig. 3a). The afternoon decay is irregular and occurs in cascades. The day of March 18 has a very low diurnal maximum (30 TECU), a decrease of − 70%. It is identical to all three stations. The recovery phase is rapid since the level of 105 TECU is present from March 20. The arrival of the magnetic disturbance on March 22 is localized at the beginning of the night. It results in a positive storm

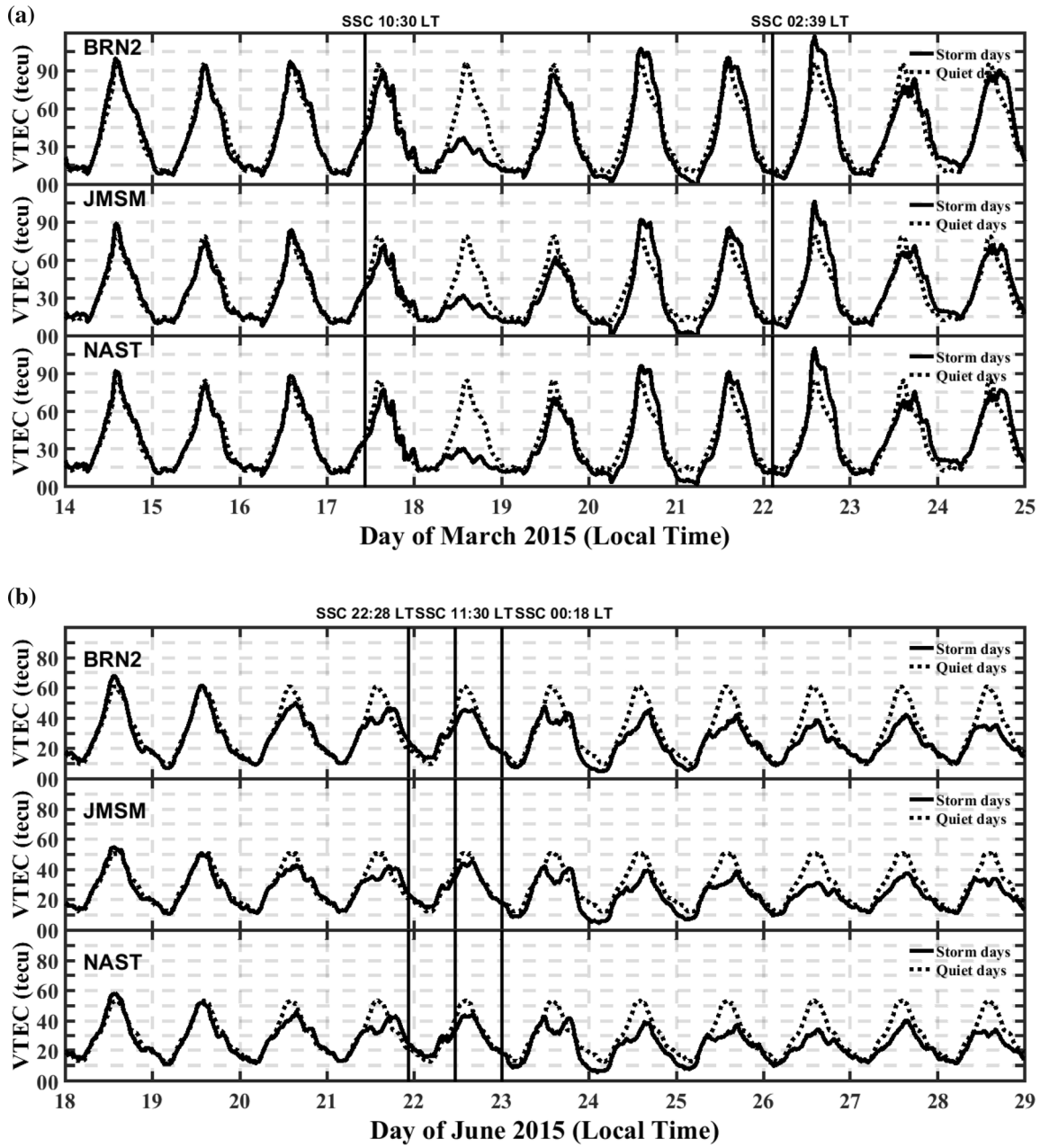

Fig. 3 (**a**–**d**) Variation of VTEC during geomagnetic storm of the period March 14–24, 2015, June 18–28, 2015, May 24–June 3, 2017, and September 3–13, 2018 (doted curves) and quiet days (solid curves), respectively

with a single peak at 120 TECU (+ 20%), followed by a slight negative phase on 23/03.

- *June 2015* This storm is located in the summer, with lower daytime values than the March equinox of the same year. Over the 4 days preceding the storm, the diurnal maximum of the VTEC decreased regularly from 70 to 45 TECU (Fig. 3b). The TEC is already below our reference over the last 2 days (20–21/06) of the quiet period. The first shock wave was localized at the beginning of the night of 22/06. It does not modify the diurnal variation of 22/06, which remains below this reference. The following days do not show any significant variations, except that one can observe a regular decrease of the diurnal maximum until a minimum on 26/06 (for example, from 49 to 31 TECU for JMSM). We can note a double peak on June 23 at all three stations, as well as low values on June 23 and 24 (5 TECU or − 50%).
- *May 2017* It is again a summer storm but located in the descending phase of the solar cycle, so the VTEC

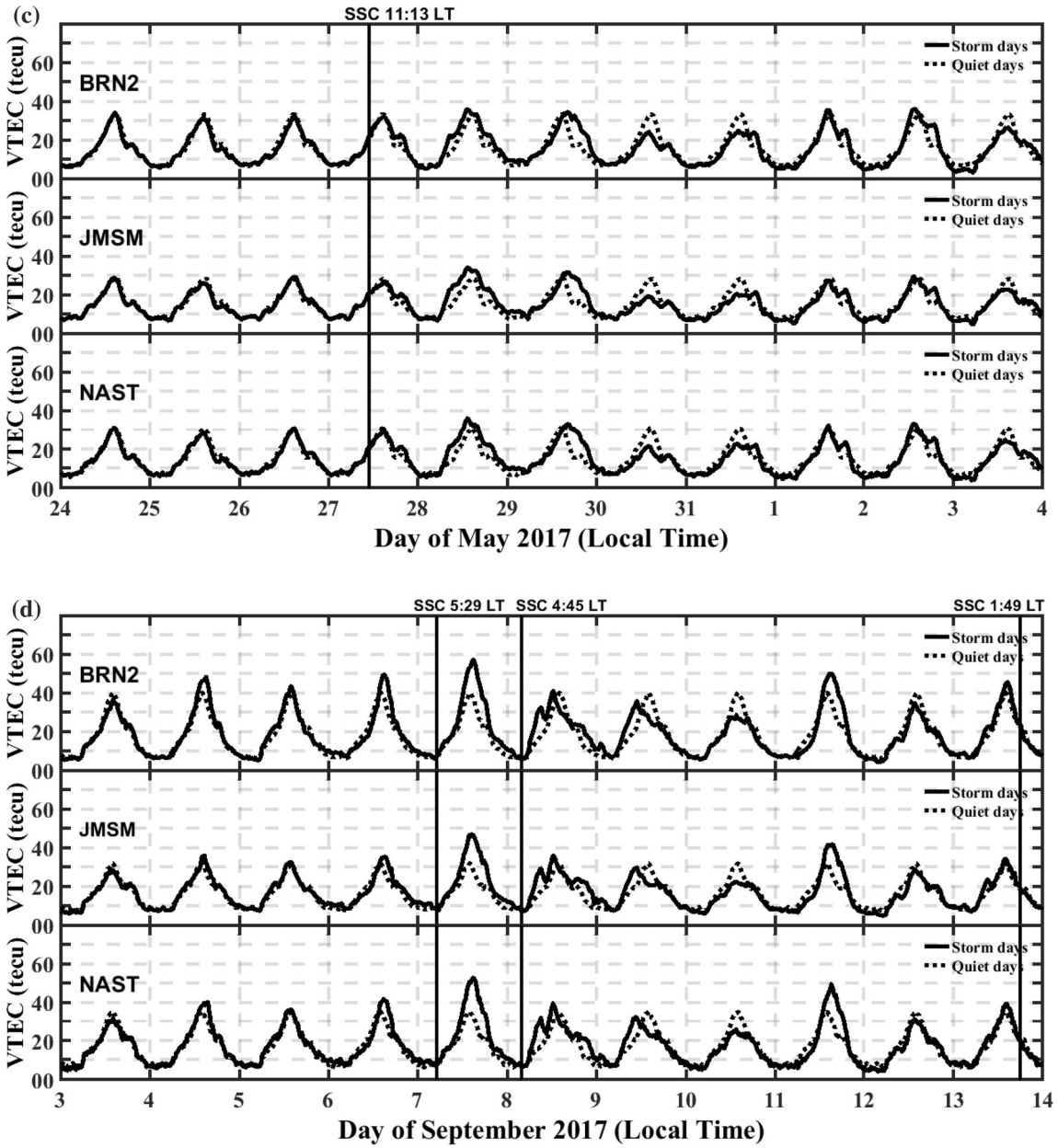

Fig. 3 continued

values are lower than in 2015, around 30 TECU by day and 10 TECU at night (Fig. 3c). The start of the magnetic storm is in the late morning of 27/05. The VTEC is slightly higher than our reference on 28 and 29/05, from 3 to 5 TECU, or + 10%. It becomes lower only late, in the recovery phase on 30 and 31/05, with a maximum of 20 TECU (− 30%).

- *September 2017* The period is again in 2017, but at the autumn equinox, so with higher VTEC values than in summer. The reference is between 10 TECU at night and a maximum of 40 TECU during the day (Fig. 3d). The start of the storm was late at night (05:29 LT) on 07/09. VTEC increases rapidly toward the daytime maximum of 14 LT at 50–60 TECU (+ 45%) depending on the station so this is a positive storm. Four days after (10/09), the VTEC is lower by − 8 TECU (30%), followed by a new positive effect on 11/09. With this long delay, it is difficult to make a link between the magnetic storm and the second storm, which began on September 12 at 20:04 TU.

3.3. Satellite data

Figure 4 (a), (b), (c), and (d) shows the global variation of the thermospheric O/N_2 ratio, obtained from the Global Ultraviolet Imager Thermosphere-Ionosphere, Mesosphere Energetics and Dynamics (GUVI-TIMED) during the four geomagnetic storms: March 16 to March 21, 2015, June 20 to June 25, 2018, May 26 to May 29, 2017, and September 6 to September 10, 2017.

At the location of the Nepalese GPS station JMSM, we observe the following behavior in the satellite data:

- For the storm of March 2015, on March 18, a significant decrease in the ratio of O/N_2 is noticed.
- For the storm of June 2015, the O/N_2 ratio started decreasing on June 22nd and became intense on June 23rd.
- For the storm of May 2017, no clear signature of change is noticed in the O/N_2 ratio.
- For the storm of September 2017, a significant enhancement in the ratio of O/N_2 is observed on September 8 and 9.

After all the geomagnetic storms, the thermospheric composition ratio of O/N_2 returned to its normal profile. For all the storms, the Global Ultraviolet Imager (GUVI) satellite O/N_2 ratio exhibits the same behavior as the VTEC measured from the ground-based GPS stations. We observed negative storms for March 2015 and June 2015, and a positive storm for September 2017. For the storm of May 2017, the change in VTEC is positive and very weak, and on satellite data, the change in O/N_2 is not very clear.

3.4. Comparison between GPS derived VTEC and CODE and IGSG models

For the four selected storms, we have represented in Fig. 5(a, b, c, d) the three variations of the VTEC (1) resulting from our RINEX processing in the form of a continuous line in black, (2) calculated by the GIM/CODE model by a square (1 point every hour), and (3) estimated by the IGSG model by an asterisk (1 point every 2 h). In each figure, we have three panels, correspondingly, from top to bottom, for BRN2, JMSM, and NAST. We have again recalled the hourly position of the shock waves with a vertical red line. To quantify the difference between our modeling and the two GIM maps, we have retained the maximum daily difference. Table 3 presents these differences for the March 2015 storm (Table 3a) and that of September 2017 (Table 3b) and for the three stations. The values are small and insignificant for the two other storms of June 2015 and May 2017, so they are not reported.

The comparisons for each storm are as follows:

- *March 2015* The three days preceding the storm (14–16/03) are characterized by higher day values than those of the two GIM models of around 10–15 TECU, i.e., + 15%. All the following days, constituting the storm period and the return phase, are well restored in time and level by the two models. During the 22/03 recovery and positive phases, we find the initial observations with day values of the two models clipped compared to our model in an identical order of magnitude of 10–15 TECU. During March 2015, the negative ionospheric storm in Nepal took place in the main phase, and it continued during the recovery phase on March 18–19. During the main and recovery phases, the diurnal variation of TEC shows wave-like oscillations. This may be due to Prompt Penetration of Electric Field (PPEF), traveling ionospheric disturbances, or by other sources. The suppression in TEC during the recovery phase was attributed to the change in the composition of the neutral gas, which decreased the O/N_2 ratio [21]. Astafyeva et al. [22] pointed out that the second IMF Bz lasted longer during the present storm and caused a more complex effect. They investigated the O/N_2 ratio changes during this geomagnetic storm using GUVI-TIMED satellite measurements and confirmed strong O/N_2 composition changes. Ramsingh et al. [23] investigated the ionospheric response due to the St. Patrick's Day's storm on March 17, 2015, in the Indian and Indonesian sectors. They suggested that the F region disturbances during the main phase were produced by PPEF.
- *June 2015* The diurnal variation of the VTEC presents high levels at the beginning of the period and a fairly regular decrease during the 10 days with either a single maximum peak or a double peak. The main conclusion is that, despite this daily variability, the two GIM models show a very strong correlation with our representation: the differences are less than 2 TECU.

During June 2015, no increase or decrease in TEC variations was observed at the Nepalese stations before or after the main phase and recovery phase of the storm. Pre-reversal enhancement (PRE) is noticed at each station during the evening time. Wave-like characteristics with a noon bite pattern were noticed during the pre-storm and post-storm of the mid-diurnal TEC. To investigate the temporal and latitudinal variation of TEC using a GPS TEC map during the storm of June 22–24, 2015, Singh and Sripathi [24] found that on June 22, Equatorial Ionization Anomaly (EIA) was suppressed and partially shifted to the Northern Hemisphere up to 0°–35° geographic latitude at 11:00–17:00 LT. The suppression of EIA, the absence of crest formation, and the negative storm effects were due to the westward electric field (reversed electrojet). They also

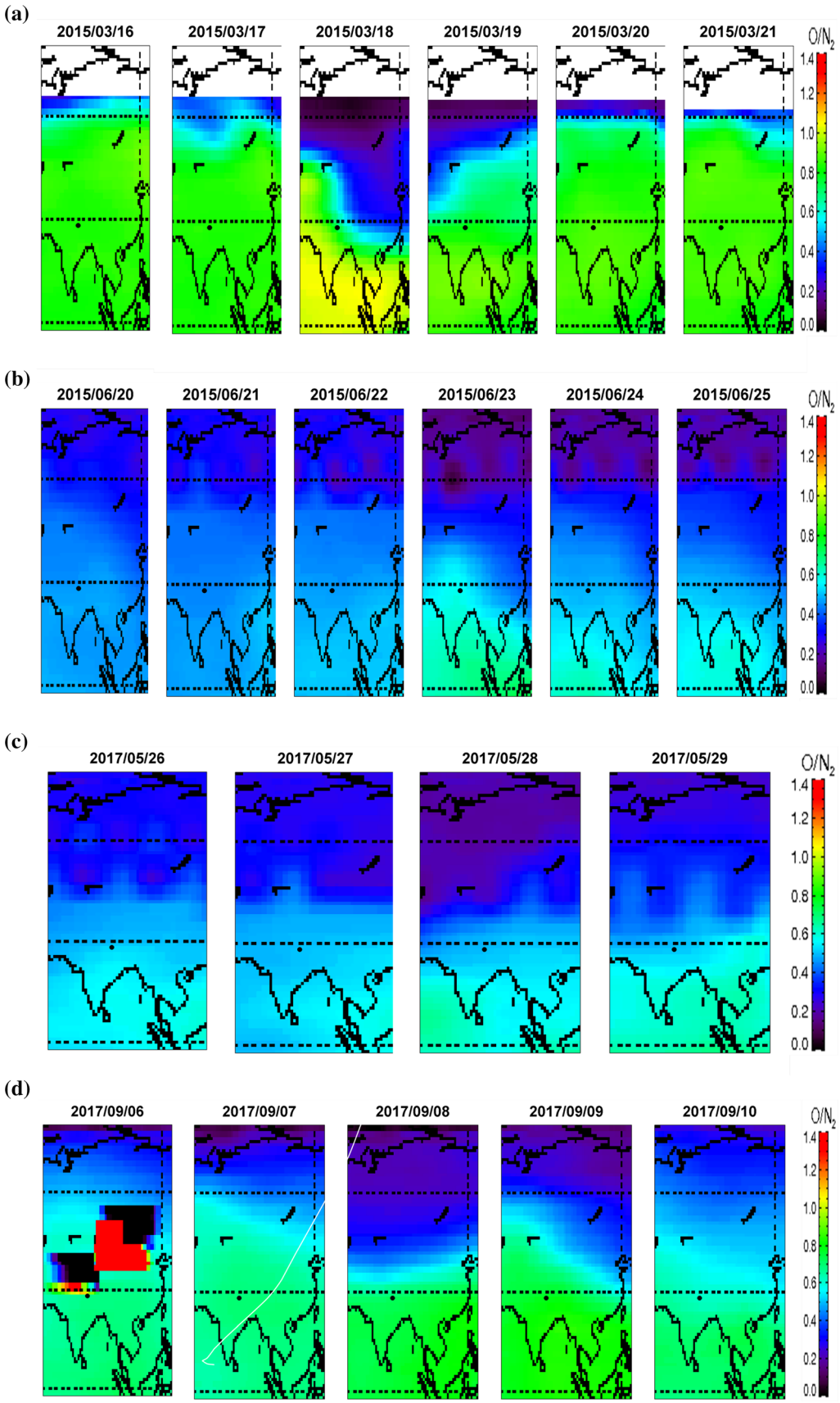
(a)
2015/03/16
2015/03/17
2015/03/18
2015/03/19
2015/03/20
2015/03/21
O/N2
1.4
1.2
1.0
0.8
0.6
0.4
0.2
0.0
(b)
2015/06/20
2015/06/21
2015/06/22
2015/06/23
2015/06/24
2015/06/25
O/N2
1.4
1.2
1.0
0.8
0.6
0.4
0.2
0.0
(c)
2017/05/26
2017/05/27
2017/05/28
2017/05/29
O/N2
1.4
1.2
1.0
0.8
0.6
0.4
0.2
0.0
(d)
2017/09/06
2017/09/07
2017/09/08
2017/09/09
2017/09/10
O/N2
1.4
1.2
1.0
0.8
0.6
0.4
0.2
0.0

◀**Fig. 4** (**a–d**) The thermospheric O/N_2 ratio obtained from the GUVI/TIMED during geomagnetic storm of the period March 16–21, 2015, June 20–25, 2015, May 26–29, 2017, and September 6–10, 2018, respectively. The black dot in each panel represents the location of JMSM station

found the suppression of EIA and negative ionospheric storms on June 24 in the Northern hemisphere due to strong westward Disturbance Dynamo Electric Fields (DDEFs). Hemispheric asymmetry in ionospheric response was noticed in the period from the initial phase to the main phase of the storm of June 2015 in both TEC maps and GNSS TEC data by Senturk [25]. Negative phases of the ionospheric storm were seen in the northern latitudes (summer hemisphere), whereas strong positive phases of the ionospheric storm were seen in the southern latitudes (winter hemisphere). The storm of June 2015 occurred on the June solstice, so dominant summer-to-winter circulation [6] and seasonal effects [26] could dominate the hemispheric asymmetry of TEC responses. The negative phase were observed during the 23 June is consistent with TEC maps of their study.

- *May 2017* The conclusion is very close to the previous case. However, the two GIM models give higher levels of 5 TECU during the high values of the VTEC of 29/05. The result is reversed at night (-4 TECU on the night of 30–31/05). The daily differences are greatest for the BRN2 station, which is closest to the dip equator compared to the two other stations (JMSM and NAST). During May 2017, an increase in VTEC in Nepal was noticed during the main phase of the storm on May 28, which gradually decreased during the post-recovery phase on May 30. This storm was studied by Lui et al. [27] and found to have increased VTEC by 120% during the main phase of the storm on May 28 due to the southward turning of IMF Bz and eastward penetration of the electric field. On May 30, over the Asian sector, nearly 2 days after the main phase, a negative storm was identified due to thermospheric composition changes, i.e., a decrease in the O/N_2 ratio. An increase in TEC due to PRE is observed during the evening time in the diurnal plot.
- *September 2017* When the diurnal maximum is between 30 and 40 TECU, the GIM modeling is correct. The difference becomes negative above 50 TECU, i.e., it peaks down to -10 TECU (BRN2 and NAST on 07/09). The strongest differences are observed with the IGSG model, on BRN2, which is of lower latitude. The lowest VTEC values were observed on 10/09 on the three curves. Over the 10 days, there is little difference in the night values. In

Table 2 Characteristics of Geomagnetic storms of March 2015, June 2015, May 2017, and September 2017 of solar cycle 24

Date	SSC	Season	Event started local time in Nepal	Case	Dst	SYM-H	Kp	AE
March 2015	March 17 04:45 UT and March 21 20:54 UT	Equinox	LT = 4.45 + 5.45 = 10 h 30 min	CME + HSSW	− 225 nT	− 250 nT	8	2000 nT ~ 12:00 UT on March 17, 2015
June 2015	June 21 16:43 UT June 22 05:45 UT and June 22 18:33 UT	Summer Solstice	Last SSC LT = 18.33 + 5.45 = 0 h 18 min	CME + HSSW	− 207 nT	− 275 nT	8	2800 nT ~ 18:00 UT on June 22, 2015
May 2017	May 27 15:28 UT	Summer Solstice	LT = 15.46 + 5.45 = 21 h 13 min	CME	− 125 nT	− 150 nT	7	2100 nT ~ 06:00 UT on May 28, 2017
September 2017	September 6 23:44 UT September 7 23:00 UT September 12 20:04 UT and September 14 23:48 UT	Equinox	First SSC LT = 23.73 + 5.45 = 5 h 33 min	CME	− 142nT	− 150 nT	8	2600 nT ~ 14:00 UT on September 8, 2017

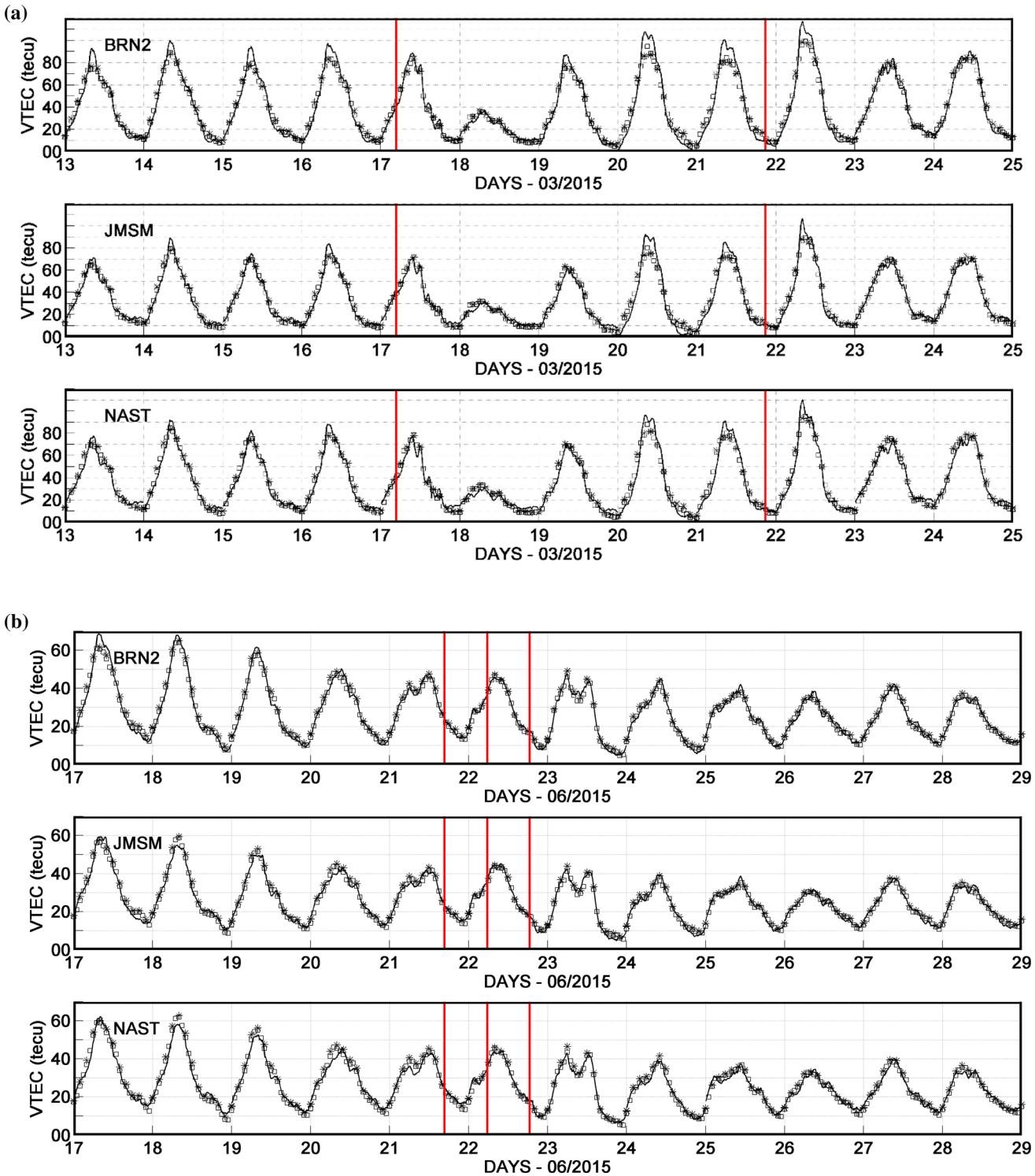

Fig. 5 (**a**–**d**) Variations of VTEC observed from GPSTEC, CODE, and IGSG for JMSM, NAST and BRN2 for three Nepalese stations during geomagnetic storm of the period March 14–24, 2015, June 18–28, 2015, May 24–June 3, 2017, and September 3–13, 2018, respectively. The solid black line on each panel represents GPSVTEC variation, whereas the black square with white background curve represents CODE and the variation in IGSG is represented by black asterisks curve

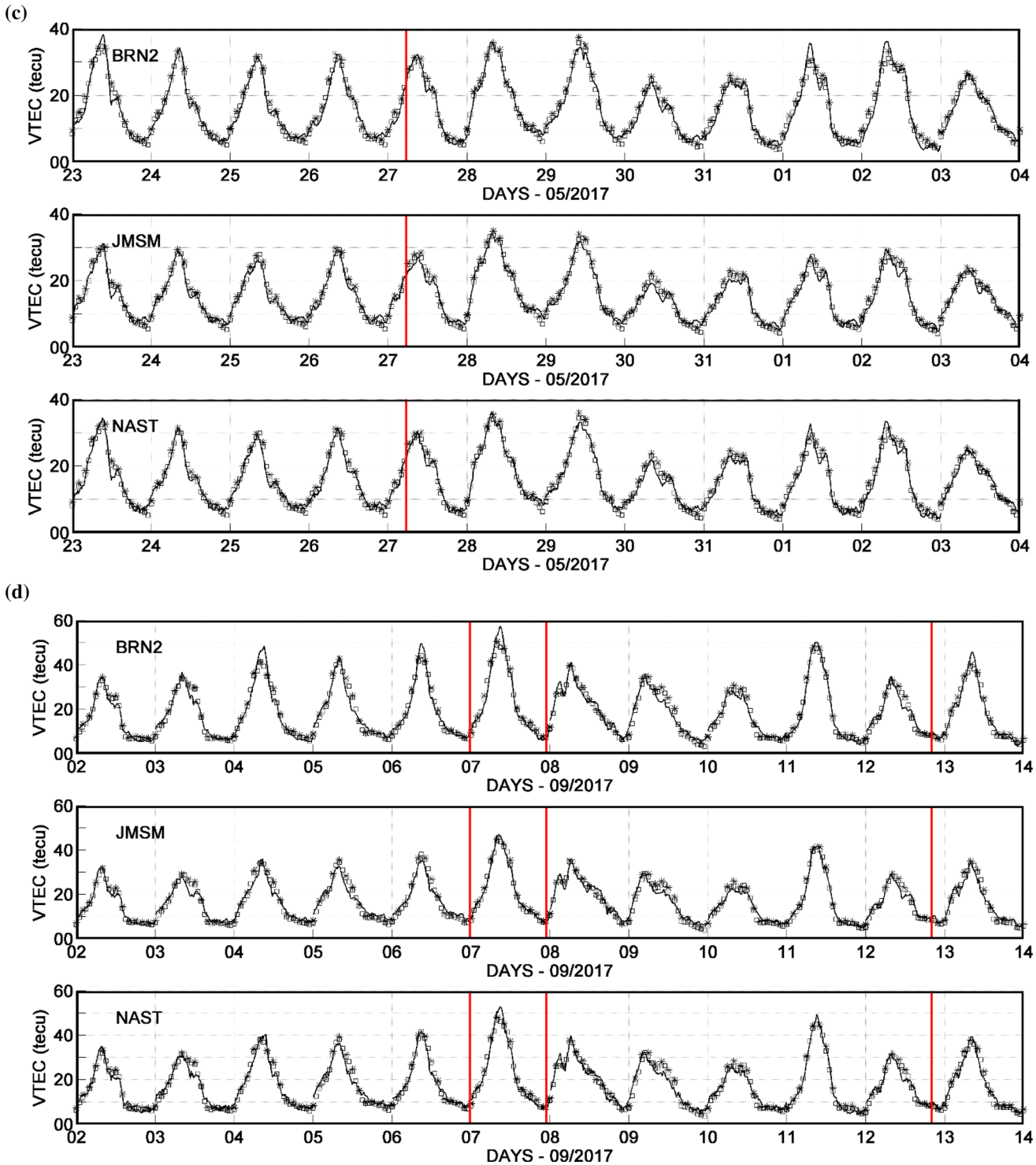

Fig. 5 continued

Table 3 Difference in RINEX VTEC for three Nepalese GPS stations JMSM, NAST, and BRN2 (a) with CODE and IGSG during geomagnetic storm of March 14–24, 2015, (b) with CODE and IGSG during geomagnetic storm of September 3–13, 2017

Days	JMSM		NAST		BRN2	
	RINEX-CODE	RINEX-IGSG	RINEX-CODE	RINEX-IGSG	RINEX-CODE	RINEX-IGSG
(a)						
14	9	10	10	10	6	9
15	11	7	11	13	13	13
16	16	16	13	16	10	11
17	2	2	4	5	− 4	− 4
18	0	1	− 3	− 2	− 3	− 3
19	− 1	0	− 1	− 5	− 3	− 4
20	10	21	12	19	7	19
21	3	8	3	8	12	13
22	16	17	19	19	10	14
23	− 3	− 2	7	8	1	1
24	1	1	− 10	− 7	− 3	− 4
(b)						
3	− 3	− 3	3	3	− 2	− 2
4	5	5	5	12	0	9
5	− 3	− 3	0	1	− 5	− 5
6	− 5	− 2	5	7	0	2
7	3	3	8	6	2	12
8	0	− 3	0	0	1	− 10
9	− 1	0	0	− 8	0	− 7
10	− 4	− 9	− 2	− 13	0	− 5
11	0	− 2	0	0	4	14
12	− 2	− 4	3	10	− 2	0
13	0	0	5	3	0	− 2

Nepal, during the main and recovery phases of the storm of September 2017, the daytime VTEC enhancement occurs at all the stations on September 8 and 9. The wave-like variations in VTEC on September 8 might be attributed to the traveling atmospheric disturbances (TADs) generated from high latitudes due to enhanced Joule heating during the storm time [5]. On September 11, there was a significant increase in daytime VTEC compared to September 10. Lei et al. [28] observed an increase in VTEC over similar latitudes for this storm, which they attributed to an increase in eastward electric fields caused by PPEF [29] when IMF Bz was southward and the neutral wind was not greatly disturbed during the initial phase of storm. Weak VTEC depletions on September 9 and 10 could be associated with the storm time neutral composition changes that extended from high latitudes to low latitudes.

Nava et al. [30] and Kashcheyev et al. [31] studied the GUVI [O/ N_2] data for the magnetic storms of March 17 and June 22, 2015. The study carried out on a global scale shows the importance of the local time of a station at the onset of the storm. The VTEC decreases significantly in Asia during the storm of March 17, 2015, which begins at 4.45 UT, as we observed in our data in Nepal, while it increases in America. Regarding the storm of June 22, 2015, which begins at 18:33 UT, it is the Asian sector that observes the increase in VTEC and the American sector that observes the decrease in VTEC.

In brief, the observations from the two global ionospheric models, CODE and IGSG, are:

- give lower VTEC values (− 10 to − 20%) than at stations in Nepal if the level is above 50 TECU, which is mostly observed during magnetically quiet periods;
- give slightly lower values (− 1 to 3 TECU) at night;
- correctly restore the level during the main phases of storms, even if these are very negative;
- show a lower result at BRN2 compared to the other two stations.

The IGSG model designed to synthesize all of the GIM maps has a degraded performance compared to CODE.

The daily variations of VTEC retrieved from the CODE and IGSG models for summer (June 2015 and May 2017) and equinoctial storms (March 2015 and September 2017) found that VTEC values are lower in summer than in the equinoxes (March 2015 and September 2017). The VTEC are found to be stronger in 2015 than in 2017 because 2015 is at the beginning of the decreasing phase of the sunspot cycle 24, and the year 2017 is at the end of the decreasing phase closer to the minimum of sunspots.

Hernandez-Pajares et al. [17] found a significant error in VTEC estimation over the ocean where only a few GPS receivers are located and one-hour resolution might be the reason why it is not good enough to analyze the storm time effect in detail. Legrand and Simon [32] analyzed a series of more than one century and half years of magnetic data and found there were 67% of magnetic quiet days, and thus more than two-thirds of the time, CODE and IGSG do not represent the data of Nepal during the equinoxes. On the contrary, during the periods of magnetic activity, the storm homogenizes the ionosphere, and geographic variability no longer exists. The discrepancy in the results between observed data and model data may be due to the local effect that CODE and IGSG do not reproduce [33, 34] and to the to the longitudinal variability of the physical process. This conclusion is consistent with the results obtained by Panda et al. [35, 36]. The authors find good agreement between the calculated VTEC in October 2012 and the Global Ionospheric Model at locations near the magnetic equator, but strong differences (20 TECU or 40%) are observed at the Delhi station, which is located near the northern ridge of the equatorial anomaly. Several physical phenomena present at low latitudes, and in particular, vertical plasma drifts, have rapid longitudinal variations [37, 38], and are not reproduced by GIM models. There are already many GNSS stations at low latitudes and, in particular, on many islands. However, the densification is not homogeneous in order to understand the variability of the ionosphere in this geographic region. Action from the scientific community is necessary to increase the network and thus improve the modeling of TEC.

This study showed that the difference between VTEC RINEX and the VTEC models is greater during the magnetic quiet days. This means that during the periods of magnetic quiet, there is wide geographic variability. There are very few geodetic stations used by CODE in the geographic vicinity of Nepal. This situation may explain the differences observed on the TEC between local measurements and global-scale modeling.

4. Conclusion

In this paper, we have attempted to reveal the impact of the intense geomagnetic storm of solar cycle 24 on VTEC over Nepal and compared the VTEC RINEX observations profile with models CODE and IGSG. The VTEC observed during these periods showed positive and negative ionospheric storms after the sudden storm commencement. After analyzing the results of VTEC obtained from RINEX observations and model data from CODE and IGSG, we have found the difference in VTEC between the two global models and the results obtained from the Nepalese GPS stations are significant beyond 5 TECU in absolute values. The second point is that the signatures in the VTEC noon bite out profile with a predominance of morning and afternoon peaks, and the nighttime peak was not clearly noticeable in the two models' representations. The discrepancies in the result between observed data and model data could be due to the local effect and also to the longitudinal variability of the physical process that the models do not produce. Therefore, the implantation of some Nepalese GPS stations in the global modeling could improve the evolution of the VTEC because the current differences are significant.

Acknowledgements The authors wish to thank high-resolution OMNI (https://omniweb.gsfc.nasa.gov) for providing 1-min-averaged field/plasma data sets; the ISGI (http://isgi.unistra.fr) for the auroral indices (AE, AU, AL, AO) and Polar cap indices (PCN and PCS) data; UNAVCO (http://www.unavco.org/data/data.html) for GPS observables; NGS, National Geodetic Survey (http://www.ngs.noaa.gov/CORS/Gpscal.shtml) for converting a calendar date to either day of year or GPS week. We finally appreciate The Astronomical Institute of the University of Bern (AIUB, Bern, Switzerland)/, The Center for Orbit Determination in Europe (CODE), http://www.aiub.unibe.ch/download/CODE for GIM/CODE data and The Crustal Dynamics Data Information System (NASA/CDDIS), https://cddis.nasa.gov/archive/gnss/products/ionex/ for GIM/IGSG data. The authors are grateful to Global UltraViolet Imager (http://guvitimed.jhuapl.edu) for making available images of thermospheric O/N_2 ratio from satellite data and CELESTRAK (https://celestrak.com/GPS/almanac/Yuma/) for GPS Yuma Almanacs data for calculating the orbit of satellite. Authors have not used any private data for this study. The author would like to acknowledge Nepal Academy of Science and Technology (NAST), Nepal for proving PhD scholarship and ICTP, Italy, for giving the opportunity to participate in a workshop on Space weather effects on GNSS operations at low latitudes.

References

[1] W D Gonzalez, J A Joselyn, Y Kamide, H W Kroehl and G Rostoker *J. Geophys. Res.* **99** 5771 (1994)
[2] M Sugiura *Hourly Values of Equatorial Dst for the IGY* (Greenbelt, Maryland, United States: NASA Goddard Space Flight Center) (1963)
[3] J W Dungey *Phys. Rev. Lett.* **6** 47 (1961)

[4] (eds.) C I Meng, M J Rycroft and L A Frank *Auroral Physics* (Cambridge, UK: Cambridge University Press) (1991)
[5] T J Fuller-Rowell, M V Codrescu, R J Moffett and S Quegan *J. Geophys. Res.* **99** 3893 (1994)
[6] T J Fuller-Rowell, M V Codrescu, H Rishbeth, R J Moffett and S Quegan *J. Geophys. Res. Space Phys.* **101** 2343 (1996)
[7] V M Vasyliunas *Particles and Fields in the Magnetosphere*, (ed.) B M McCormac (New-York: Springer) p 60 (1970)
[8] M Blanc and A D Richmond *J. Geophys. Res.* **85** 1669 (1980)
[9] Y Huang, S Yang, Y Qiao, M Lin, B Zhao, and K Tan *Geod. Geodyn.* **8** 285 (1017)
[10] B Adhikari, S Dahal, M Karki, R K Mishra, S Sasmal and V Klausner *Geoenviron. Disasters* **7** 1 (2020)
[11] K Ansari, S K Panda and P Jamjareegulgarn *Acta Astronaut.* **169** 216 (2020)
[12] P Jamjareegulgarn, K Ansari and A Ameer *Acta Astronaut.* **177** 497 (2020)
[13] D Pandit, B Ghimire, C Amory-Mazaudier and R Fleury *Ann. Geophys.* **39** 743 (2021)
[14] B Hofmann-Wellenhof, H Lichtenegger and J Collins *Global Positioning System: Theory and Practice* (Wien, Austria: Springer) (1992)
[15] S Schaer *Doctoral dissertation* (*Bern University*, Bern) (1999)
[16] I Azzouzi, Y Migoya-Orue, C Amory-Mazaudier, R Fleury, S M Radicella and A Touzani *Adv. Space Res.* **56** 2040 (2015)
[17] M Hernandez-Pajares, J M Juan, J Sanz, R Orus, A Garcia-Rigo, A Komjathy, S Schaer and A Kranskowski *J. Geod.* **83** 263 (2009)
[18] P Chen and H Liu *Space Res.* **65** 163 (2020)
[19] M Hernández-Pajares, D Roma-Dollase, A Krankowski, R Ghoddousi-Fard, Y Yuan, Z Li, H Zhang, C Shi, J Feltens, A Komjathy, P Vergados, S Schaer, A Garcia-Rigo and J M Gmez-Cama In: *IGS Workshop 2016, 8–12 Feb, Sydney, Australia* (2016)
[20] D Roma-Dollase *Doctoral Dissertation* (Universitat Politècnica de Catalunya, Spain) (2019)
[21] R de Jesus, Y Sahai, P R Fagundes, A J de Abreu, C Brunini, M Gende and J A Bittencourt *Space Res.* **52** 147 (2013)
[22] E Astafyeva, I Zakharenkova and M Förster *J. Geophys. Res. Space Phys.* **120** 9023 (2015)
[23] S S Ramsingh, S Sreekumar, S Banola, K Emperumal, P Tiwari and B S Kumar *J. Geophys. Res. Space Phys.* **120** 10864 (2015)
[24] R Singh and S Sripathi *J. Geophys. Res. Space Phys.* **122** 11 (2017)
[25] E Sentürk *Astrophys. Space Sci.* **365** 1 (2020)
[26] H Kil *J. Geophys. Res.* **111** A12311 (2006)
[27] L Liu, S Zou, Y Yao and E Aa *GPS Solut.* **24** 1 (2020)
[28] J Lei, F Huang, X Chen, J Zhong, D Ren, W Wang et al *J. Geophys. Res. Space Phys.* **123** 3217 (2018)
[29] N Balan, Y Otsuka, M Nishioka and J Y Liu *J. Geophys. Res. Space Phys.* **118** 2660 (2013)
[30] B Nava, J Rodríguez-Zuluaga, K Alazo-Cuartas, A Kashcheyev, Y Migoya-Orué, S M Radicella and C Amory-Mazaudier *J. Geophys. Res. Space Phys.* **121** 3421 (2016)
[31] A Kashcheyev, Y Migoya-Orué, C Amory-Mazaudier, R Fleury and B Nava *J. Geophys. Res. Space Phys.* **123** 5000 (2020)
[32] J P Legrand and P A Simon *Ann. Geophys.* **7** 565 (1989)
[33] N Matuura *J. Geophys. Res.* **79** 4679 (1974)
[34] C Zoundi, O Frederic, N Emmanuel, R Fleury and Z Francois *Eur. Sci. J.* **9** 74 (2013)
[35] S K Panda, S S Gedam and G Rajaram In *2013 IEEE International Geoscience and Remote Sensing Symposium-IGARSS* 1839 (2013)
[36] (eds.) S K Panda, S S Gedam and S Jin *Satellite Positioning—Methods, Models and Applications* (London, UK: IntechOpen) (2015)
[37] B G Fejer, D T Farley and C A Gonzales *J. Geophys. Res. Space Phys.* **86** 215 (1981)
[38] B G Fejer, E R De Paula, S A Gonzalez and R F Woodman *J. Geophys. Res. Space Phys.* **96** 13901 (1991)

Publisher's Note Springer Nature remains neutral with regard to jurisdictional claims in published maps and institutional affiliations.

Springer Nature or its licensor holds exclusive rights to this article under a publishing agreement with the author(s) or other rightsholder(s); author self-archiving of the accepted manuscript version of this article is solely governed by the terms of such publishing agreement and applicable law.